Revisiting the energy efficiency and (potential) full-cell performance of lithium-ion batteries employing conversion/alloying-type negative electrodes

Jakob Asenbauer [a,b], Alberto Varzi [a,b], Stefano Passerini [a,b], Dominic Bresser [a,b,*]

[a] Helmholtz Institute Ulm (HIU), Helmholtzstrasse 11, 89081, Ulm, Germany
[b] Karlsruhe Institute of Technology (KIT), P.O. Box 3640, 76021, Karlsruhe, Germany

HIGHLIGHTS

- Critical analysis of the energy efficiency for conversion/alloying anodes (CAMs).
- Evaluation of important impact factors such as the conversion/alloying ratio.
- Demonstration of the beneficial effect of capacity-limited cycling and prelithiation.
- Proof-of-concept that energy efficiencies of more than 95% are feasible for CAMs.

GRAPHICAL ABSTRACT

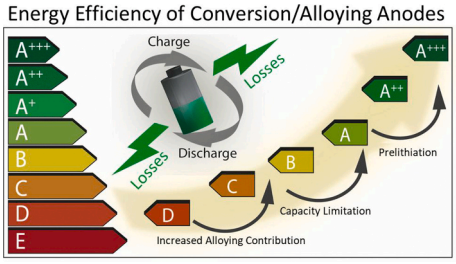

ARTICLE INFO

Keywords:
Energy efficiency
Conversion: alloying
Lithium-ion anode
Battery

ABSTRACT

The energy efficiency of new lithium-ion chemistries is a very important, but frequently not provided performance measure for new alternative active materials for application as negative and positive lithium-ion battery (LIB) electrodes. This is particularly true for those active materials, not hosting lithium cations via insertion mechanisms, but via alloying and/or conversion reactions.

Herein, the energy efficiency of alternative negative electrode active materials hosting lithium via combined conversion and alloying processes and the impact factors on the energy efficiency of such compounds in complete battery cells (full-cells) is revisited. Specifically, the effect of (i) varying the relative contribution of the conversion and alloying reaction, (ii) limiting the specific capacity, (iii) pre-cycling and pre-lithiating the anode, as well as (iv) the choice of the active material for the positive electrode, is investigated. The results show that a proper combination of these measures may enable lithium-ion cells based on conversion/alloying anodes that provide energy efficiencies of >95%, accompanied by gravimetric energy densities that might outperform graphite-based lithium-ion cells.

1. Introduction

The continuously rising importance of lithium-ion batteries for a wide range of applications, including portable electronics, power tools, (hybrid) electric vehicles, and stationary storage, is triggering increasing needs for new electrode active materials capable of hosting more lithium

* Corresponding author. Helmholtz Institute Ulm (HIU), Helmholtzstrasse 11, 89081, Ulm, Germany.
E-mail address: dominic.bresser@kit.edu (D. Bresser).

ions per unit weight and volume than conventional insertion-based electrodes, thus allowing for further increasing energy densities [1–8]. In this regard, conversion materials have attracted great interest as they allow for very high lithium uptake in the form of, e.g., Li_2S or Li_2O in the lithiated state – starting from elemental sulfur [9,10] or oxygen [11–13] at the positive electrode or transition metal oxides [14–17] at the negative electrode. This outstanding lithium storage capability, however, comes with several challenges related to the formation of these new chemical species as well as the extensive bond cleavage and formation required. Beside extensive volume variations, the formation of rather insulating compounds, and the potentially challenging reversibility of the de-/lithiation reaction, a major challenge is the difference in (average) voltage for the lithiation and delithiation reactions – commonly referred to as voltage hysteresis [16–19]. A pronounced voltage hysteresis, in fact, limits the achievable energy efficiency [20–22] and leads to significant heat evolution [23]. The origin of this voltage hysteresis for conversion transition metal oxides as alternative anodes is not yet fully understood, though it has been suggested that it might be related to different reaction pathways for the lithiation and subsequent delithiation [23–25] rather than "simple" kinetics. These, in fact, could be overcome by applying elevated temperatures or the realization of extremely short electron and Li^+ ion transport pathways [25–27]. The observation that the choice of the anion (i.e., oxides vs., e.g., phosphides, nitrides, or hydrides) plays a decisive role for the magnitude of the voltage hystereses does, in fact, point in the same direction [28].

In an attempt to address this issue for oxides, which are easy to handle and synthesize, researchers introduced alloying elements, such as zinc or tin, into conversion-type active materials, as these can add to the achievable capacity and are commonly characterized by smaller voltage hystereses, though still larger than for insertion- and intercalation-type materials (e.g., graphite) [17,21,29–32]. Simultaneously, the incorporation into conversion-type active materials is considered to buffer the extensive volume variations occurring for pure alloying compounds, while the upon lithiation formed transition metal nanograins may favor the electronic conductivity and, thus, the overall reaction kinetics [17,33]. Following this approach, we designed inter alia transition metal (TM) doped ZnO ($Zn_{1-x}TM_xO$) as alternative anode materials [34,35], targeting a rather high relative contribution of the alloying reaction. Very recently, we have shown that such materials (exemplarily illustrated for $Zn_{0.9}Fe_{0.1}O$) may, indeed, be employed in highly efficient lithium-ion cells, using $LiNi_{0.5}Mn_{1.5}O_4$ for the positive electrode, with an energy efficiency as high as 93% [36]. This value is comparable to state-of-the-art lithium-ion battery cells comprising graphite-based negative electrodes [21,37].

Herein, we carefully analyze under which conditions conversion/alloying materials (CAMs) can provide such competitive energy efficiencies (EEs), in particular, the energy loss and the effect of the abovementioned measures on it, as a function of different cathode chemistries. Finally, we provide a rough calculation of the impact of the EEs on commercial scale batteries.

2. Theoretical basics

The energy efficiency of a lithium-ion cell (or a battery cell in general) is the product of two different contributions: The first one, commonly reported in scientific studies, is the coulombic efficiency (CE). The CE of a material or a cell indicates the fraction of charge reversibly stored in an electrode (or cell). Irreversible processes commonly comprise the decomposition of the electrolyte at the electrode/electrolyte interface or the electrochemically driven degradation of the electrode active materials. Accordingly, the CE is essentially the ratio of the delivered capacity upon discharge and the capacity supplied upon charge, as described in Equation (1):

$$CE = \frac{\int_0^{t_d} I_d(t)dt}{\int_0^{t_c} I_c(t)dt} = \frac{Q_d}{Q_c} \quad (1)$$

where I_d/I_c represents the discharge/charge current and t_d/t_c the discharge/charge time. It should be noted at this point that the term is reversed when studying anode material candidates in half-cell configuration, as the irreversible reactions are essentially occurring upon lithiation (i.e., the discharge in such configuration, since the lithium metal counter electrodes serves as the negative electrode in that case), while the reversible capacity is obtained upon delithiation (i.e., the charge in that case).

The second important contribution is the voltage efficiency (VE), which is a direct measure of the aforementioned voltage hysteresis, originating inter alia from polarization and overpotential effects or different reaction pathways for the lithiation and delithiation. Therefore, VE values different from unity might originate from thermodynamic and kinetic impact factors. The VE is expressed as:

$$VE = \frac{\frac{\int_0^{t_d} U_d(t)dt}{t_d}}{\frac{\int_0^{t_c} U_c(t)dt}{t_c}} = \frac{\overline{U}_d}{\overline{U}_c} \quad (2)$$

where U_d and U_c represent the cell voltage during discharge and charge and $\overline{U}_d$ and $\overline{U}_c$ are the average discharge and charge voltage, respectively. The product of CE and VE yields the overall energy efficiency (EE), i.e., the ratio of the energy released from the battery cell (E_{out}) upon discharge over the energy inserted (E_{in}) upon charge:

$$EE = \frac{E_{out}}{E_{in}} = \frac{\int_0^{t_d} U_d(t)I_d(t)dt}{\int_0^{t_c} U_c(t)I_c(t)dt} \quad (3)$$

In the case of a constant current, Equations (1) and (3) can be simplified to Equations (4) and (5), respectively:

$$CE = \frac{I_d t_d}{I_c t_c} \quad (4)$$

$$EE = \frac{I_d \int_0^{t_d} U_d(t)dt}{I_c \int_0^{t_c} U_c(t)dt} \quad (5)$$

Combining Equations (4) and (5) then yields Equation (6), which nicely illustrates the abovementioned relation between the EE, CE, and VE.

$$EE = CE\frac{\frac{\int_0^{t_d} U_d(t)dt}{t_d}}{\frac{\int_0^{t_c} U_c(t)dt}{t_c}} = CE\frac{\overline{U}_d}{\overline{U}_c} = CE^*VE \quad (6)$$

3. Experimental section

3.1. Materials synthesis

In order to analyze the impact of varying the contribution of the alloying reaction, we evaluated a series of CAMs that have been reported earlier and were synthesized accordingly, i.e., carbon-coated $ZnFe_2O_4$ (ZFO) [38] (the carbon coating was performed according to Ref. [36]), carbon-coated $Zn_{0.9}Fe_{0.1}O$ [34,36], and carbon-coated $Sn_{0.9}Fe_{0.1}O_2$ [39]. As all materials have been coated with carbon, we will simply refer to ZFO, $Zn_{0.9}Fe_{0.1}O$, and $Sn_{0.9}Fe_{0.1}O_2$ in the following.

3.2. Electrode preparation

The electrode composition was kept constant for all CAMs in order to keep the results as comparable as possible. In all cases, sodium carboxymethyl cellulose (CMC, Dow Wolff Cellulosics) was used as binder and dissolved in ultra-pure water to obtain a 1.25% solution. The conductive carbon (Super C65, Imerys) and the active material were added, providing a total ratio of 5 wt% CMC, 20 wt% conductive carbon, and 75 wt% of the active material. The resulting slurry was homogenized via ball milling (FRITSCH Pulverisette 4) for 4 × 30 min at 400/-800 rpm with 10 min rest in between each milling cycle. Subsequently, the slurry was cast on dendritic copper foil (Schlenk). The electrode sheets were first dried at 80 °C for 15 min and then at room temperature overnight. Disc electrodes with a diameter of 12 mm were punched and dried for 12 h at 120 °C under vacuum. The average mass loading was about 1.5 mg cm ^{2}. The $LiFePO_4$ (LFP) electrodes used for the ZFO/LFP full-cells were prepared as reported by Varzi et al. [33].

3.3. Cell assembly and electrochemical characterization

For the electrochemical characterization, three-electrode Swagelok-type cells were used. All cells were assembled in an argon-filled glove box (oxygen and water content < 0.1 ppm). In the case of half-cells, battery-grade lithium metal (Honjo) served as counter and reference electrodes, while glass fiber sheets (GFA, Whatman) were used as separator. In the case of the ZFO/LFP full-cells, polypropylene membranes (Freudenberg FS 2226) were utilized as separator. A 1 M solution of $LiPF_6$ in a 3:7 vol mixture of ethylene carbonate (EC) and diethyl carbonate (DEC; UBE) was used as electrolyte. The ZFO, $Zn_{0.9}Fe_{0.1}O$, and $Sn_{0.9}Fe_{0.1}O_2$ half-cells were cycled between 0.01 and 3.0 V vs. Li^+/Li. One formation cycle at a specific current of 50 mA g ^{1} was performed prior to the constant current cycling at 100 mA g ^{1}. Capacity-limited cycling was conducted via discharging the half-cells to 0.01 V at 50 mA g ^{1} and subsequently fixing the capacity to the given value. The ZFO/LFP full-cells were cycled within a voltage range from 2.8 to 4.2 V vs. Li^+/Li at a current density of 3 mA cm ^{2} (i.e., 2.45 A g $^{1}_{ZFO}$). As all electrochemical tests were conducted using lithium metal as quasi-reference electrode, all the voltage and potential values provided herein refer to Li^+/Li. The galvanostatic cycling was conducted at 20 °C, either using a Maccor 4300 battery test system (half-cells) or a Biologic VMP3 (full-cells).

4. Results and discussion

4.1. Exemplary illustration of the EE for CAMs

In Fig. 1, we have exemplarily depicted the dis-/charge profile for a lithium-ion cell comprised of a $Zn_{0.9}Fe_{0.1}O$ anode and a theoretical LFP (LFP_{theor}) cathode with a constant de-/lithiation potential of 3.4 V, i.e., neglecting its voltage hysteresis [22]. The dis-/charge profile of the anode was, instead, obtained experimentally in half-cell tests, applying cut-off voltages of 0.01 V and 3.0 V for the lithiation and delithiation, respectively. Such high delithiation potential is not suitable for practical full-cells (though of scientific interest), but this shall be neglected for the moment as well, since the purpose of this figure is simply to illustrate the low EE's issue. The energy stored reversibly in such a partially theoretical full-cell is highlighted in green, while the energy lost is highlighted in red. It is, thus, immediately apparent that a large voltage hysteresis between the discharge (delithiation of the anode) and charge (lithiation of the anode) – i.e., a low VE – in combination with a CE of well below 100% results in a rather low EE. In the following, we will investigate different impact factors that have a substantial effect on the EE – always with a clear focus on the negative electrode active material. Factors that have essentially kinetic effects – such as the size of the active material particles (herein always in the few tens of nanometers range), the electrode composition (e.g., the ratio of the conductive carbon), the ambient temperature, and the dis-/charge rate – were kept constant in order to allow for a fair comparison.

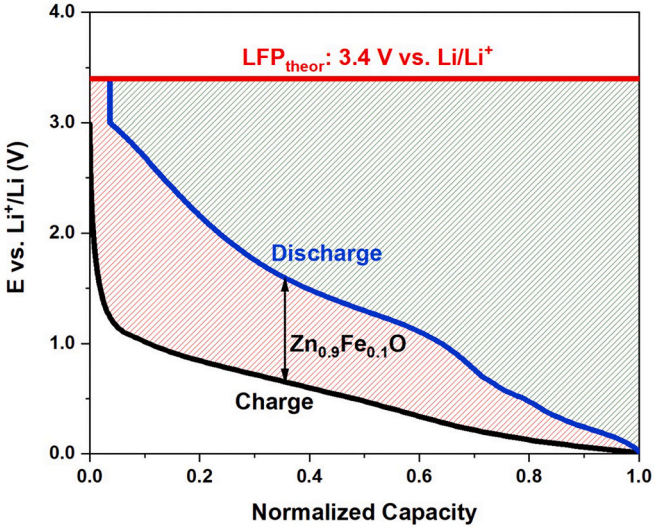

Fig. 1. Schematic illustration of the EE for a (partially) theoretical lithium-ion cell comprised of an exemplary $Zn_{0.9}Fe_{0.1}O$-based anode and a theoretical LFP (LFP_{theor}) cathode with a constant de-/lithiation potential of 3.4 V (in red). The dis-/charge profile of the anode was obtained experimentally in half-cell configuration, setting the cut-off potentials to 0.01 V and 3.0 V. The terms 'charge' (in black) and 'discharge' (in blue) refer to the illustrated full-cell design. The reversibly stored energy, equivalent to the area between the delithiation curve of the anode (in blue) and the theoretical lithiation curve of the cathode (in red) is displayed in green and the "lost" energy is depicted as the red area – being the sum of the coulombic and voltage inefficiency. (For interpretation of the references to colour in this figure legend, the reader is referred to the Web version of this article.)

4.2. The impact of the relative contribution of the alloying reaction

In a first step, we studied the impact of varying the relative contribution of the alloying and conversion reaction to the total capacity. For this purpose, we chose three different CAMs that have been previously well characterized: $ZnFe_2O_4$ (ZFO) [33,38,40–46], $Zn_{0.9}Fe_{0.1}O$ [23,34,36,47–49], and $Sn_{0.9}Fe_{0.1}O_2$ [39,50,51]. The particle size (Fig. S1), carbon coating content and specific BET surface area (Table S1) were kept as similar as possible in order to avoid any significant impact on the reaction kinetics at the given, rather low dis-/charge rates. The general reaction mechanisms are briefly recapitulated in the following to illustrate the varying ratio of the conversion and alloying reactions to the total capacity.

The relevant electrochemical processes that occur for ZFO are:

$$ZnFe_2O_4 + 8\,Li^+ + 8\,e^- \rightarrow 2\,Fe^0 + 4\,Li_2O + Zn^0 \quad (7)$$

$$Zn^0 + Li^+ + e^- \rightarrow LiZn \quad (8)$$

Accordingly, 8 Li^+ per unit formula are stored via a conversion and 1 Li^+ is stored by alloying, resulting in a relative contribution of the alloying reaction of 11.1%.

The de-/lithiation of $Zn_{0.9}Fe_{0.1}O$ occurs generally via the following reaction mechanism:

$$Zn_{0.9}Fe_{0.1}O + 2\,Li^+ + 2e^- \rightarrow 0.1\,Fe^0 + Li_2O + 0.9\,Zn^0 \quad (9)$$

$$0.9\,Zn^0 + 0.9\,Li^+ + 0.9\,e^- \rightarrow 0.9\,LiZn \quad (10)$$

Accordingly, the relative contribution of the alloying reaction is increased to 31%, i.e., about 20% higher than in case of ZFO.

For $Sn_{0.9}Fe_{0.1}O_2$, the electrochemical de-/lithiation takes place via the following reaction mechanism:

$$Sn_{0.9}Fe_{0.1}O_2 + 4\,Li^+ + 4\,e^- \rightarrow 0.1\,Fe^0 + 2\,Li_2O + 0.9\,Sn^0 \quad (11)$$

$$0.9\;Sn + 3.96\,Li^+ + 3.96\,e^- \rightarrow 0.9\,Li_{4.4}Sn \quad (12)$$

In this case, the relative contribution of the alloying reaction is further increased to 49.7%. Thus, these three materials show an alloying contribution increasing by constantly around 20% enabling a rather suitable study. The comparison of the galvanostatic cycling data for 50 cycles, all in half-cell configuration, is provided in Fig. 2. The CE is deducted from the half-cell tests, assuming a CE of 100% for the LFP_{theor} cathode, used for the calculation of the VE and EE. Generally, all half-cells reveal stable capacities and CEs of about 98% after a few cycles. The major differences are related to the VEs and, as a consequence, the EEs. For ZFO, the EE stabilizes at about 68% (Fig. 2a), while it is about 71% in case of $Zn_{0.9}Fe_{0.1}O$ (Fig. 2b) and around 74% for $Sn_{0.9}Fe_{0.1}O_2$ (Fig. 2c). Accordingly, an increase of about 20% for the alloying contribution results in an increase by 3% of the EE due to the improved VE, i.e., reduced voltage hysteresis. In detail, the average lithiation and delithiation potential for ZFO is about 0.72 V and 1.54 V, respectively, resulting in an average voltage hysteresis of 0.82 V (inset in Fig. 2a). For $Zn_{0.9}Fe_{0.1}O$, the average lithiation and delithiation potential is 0.49 V and 1.29 V, which leads to a decreased voltage hysteresis of 0.80 V (inset in Fig. 2b). In case of $Sn_{0.9}Fe_{0.1}O_2$, for which the alloying reaction contributes with almost 50% to the total capacity, the voltage hysteresis is further decreased to 0.68 V with and average delithiation potential of 1.22 V and an average lithiation potential of 0.54 V (inset in Fig. 2c). In addition, the generally lowered de-/lithiation potential with an increasing contribution of the alloying reaction has also a "mathematical" effect, since the total amount of ir-/reversibly stored energy is increasing, i.e., the green area in the corresponding plots of the dis-/charge curve, which has a kind of "diluting" effect on the calculation of the EE.

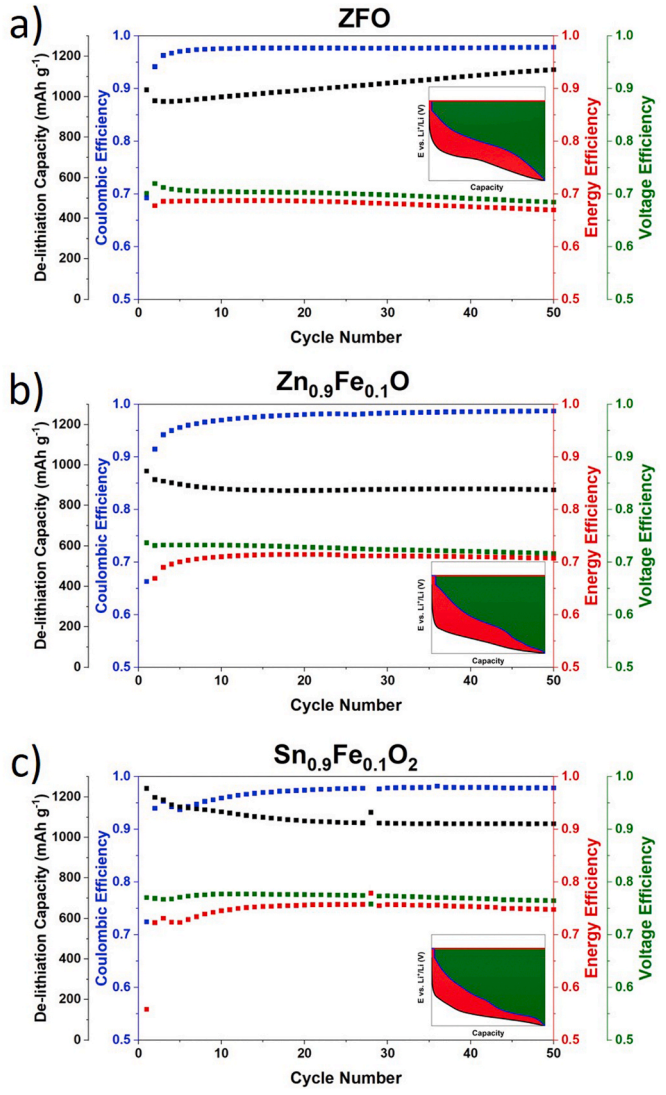

Fig. 2. Comparison of the de-/lithiation capacity, CE, VE, and EE plotted vs. the cycle number and representative dis-/charge profiles as inset for (a) ZFO, (b) $Zn_{0.9}Fe_{0.1}O$, and (c) $Sn_{0.9}Fe_{0.1}O_2$ cycled in half-cell configuration. The VE and EE were calculated employing a LFP_{theor} cathode (with a de-/lithiation potential of 3.4 V). The half-cells were cycled with a specific current of 100 mA g^{-1} after the first cycle, for which a specific current of 50 mA g^{-1} was applied.

4.3. *The impact of limiting the cycled capacity*

In a second step, the impact of capacity-limited cycling was investigated. Limiting the capacity is essentially another way to vary the relative contribution of the alloying reaction, which mainly occurs at lower potentials than the conversion reaction, even though there is some region in which both reactions are overlapping, depending also on the elemental composition of the CAM [34,38,39,46,47,50]. In order to still have a significant increase over the theoretical capacity of graphite, the capacity of the half-cells comprising $Zn_{0.9}Fe_{0.1}O$ and $Sn_{0.9}Fe_{0.1}O_2$ as working electrodes ($Zn_{0.9}Fe_{0.1}O$-Cap.Lim. and $Sn_{0.9}Fe_{0.1}O_2$-Cap.Lim., respectively) was limited to 600 mAh g ^{1}. The cycling data are displayed in Fig. 3, including the CE as determined in half-cells and the VE and EE considering a LFP_{theor} cathode. In the first cycle, the half-cells were lithiated until 0.01 V and then cycled with the aforementioned

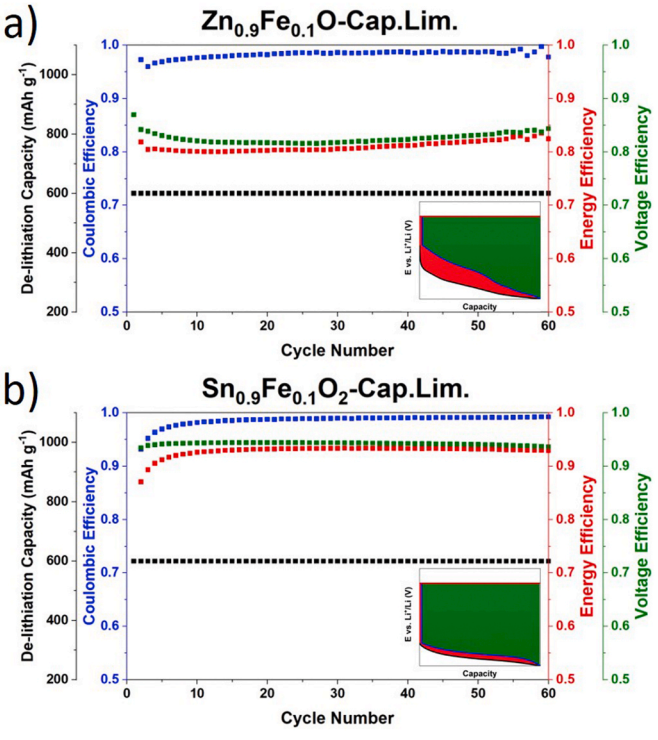

Fig. 3. Comparison of the de-/lithiation capacity, CE, VE, and EE plotted vs. the cycle number and representative dis-/charge profiles as inset for (a) $Zn_{0.9}Fe_{0.1}O$ ($Zn_{0.9}Fe_{0.1}O$-Cap.Lim.) and (b) $Sn_{0.9}Fe_{0.1}O_2$ ($Sn_{0.9}Fe_{0.1}O_2$-Cap.Lim.) cycled in half-cell configuration. The VE and EE were calculated based on a LFP_{theor} cathode (with a de-/lithiation potential of 3.4 V). The half-cells were initially discharged to 0.01 V at a specific current of 50 mA g^{-1} and then cycled with a capacity limit of 600 mAh g^{-1} at a specific current of 100 mA g^{-1}.

capacity limit. Considering the theoretical capacity of $Zn_{0.9}Fe_{0.1}O$ (966 mAh g^{-1}), the contribution of the alloying reaction is 333 mAh g^{-1}. Accordingly, the relative ratio of the alloying reaction increases from 31% to 55.5% when limiting the capacity to 600 mAh g^{-1} in the low-voltage region. As a consequence, the average EE increases from 71% to 81% thanks to a slightly enhanced CE (99%) and a greatly improved VE (83%) (Fig. 3a). This enhanced VE results from the decreased average voltage hysteresis from 0.80 V to 0.53 V (with an average lithiation and delithiation voltage of 0.47 and 1.00 V, respectively; inset in Fig. 3a). For $Sn_{0.9}Fe_{0.1}O_2$-Cap.Lim. (Fig. 3b), the improvement of the average EE is even more pronounced, i.e., from 74% to, remarkably, 93% thanks to the increased CE (99%) and VE (94%) (inset in Fig. 3b). Here, the average voltage hysteresis is only 0.20 V (with an average lithiation and delithiation voltage of 0.32 V and 0.52 V, respectively; inset in Fig. 3b) compared to 0.68 V recorded using the cut-off potentials at 0.01 V and 3.0 V (inset in Fig. 2c). In fact, the alloying contribution to the overall theoretical capacity (1477 mAh g^{-1}) of $Sn_{0.9}Fe_{0.1}O_2$ is 735 mAh g^{-1}. Thus, limiting the capacity to 600 mAh g^{-1} in the low voltage range means that only the alloying reaction occurs.

At first sight, such a capacity limitation, i.e., not using the whole capacity available, might appear detrimental for the specific energy achievable, but this is more than counterbalanced by the reduced need of cathode active material matching such high capacities available within a larger potential range [50,51]. Nonetheless, the anode would need to be pre-lithiated in such case apparently, which is a very active field of research and development in academia and industry at present – not only for batteries, but also for lithium-ion capacitors [52–57].

4.4. *The effect of pre-lithiating the anode*

For the determination of the effect of pre-lithiating the anode, we analyzed the ZFO/LFP full-cell data reported by Varzi et al. [33]. The results are presented in Fig. 4. As described in detail by Varzi et al. [33], the ZFO anodes were pre-cycled in half-cells for 20 cycles at a specific current of 100 mA g^{-1}. After lithiation to different capacity levels, 0 mAh g^{-1} (i.e., used as obtained after the 20th delithiation to 3.0 V), 200 mAh g^{-1}, or 600 mAh g^{-1} (therein abbreviated as ZFO-deLi, ZFO-200, and ZFO-600), the ZFO electrodes were assembled into ZFO/LFP full-cells. Based on an ZFO/LFP active materials' mass ratio of 0.67 and a capacity of 160 mAh g^{-1} for LFP and 1070 mAh g^{-1} for ZFO, the capacity ratios were 0.22, 0.28, and 0.51, respectively (i.e., all cells were cathode-limited). Please note, that the herein reported EEs are calculated only with respect to the anode, i.e., any energy loss due to the cathode are neglected in order to allow for a better comparison with the results for the other CAMs. Remarkably, all three cells show significantly increased EEs compared to the results provided in Fig. 2a, despite the high current applied, i.e., 2.45 A g^{-1}_{ZFO}. The two full-cells comprising ZFO-deLi and ZFO-200 as active material for the anode exhibit an average EE of 83% thanks to the enhanced average CEs (>99.7%) and VEs (83%) (Fig. 4a and b). These correspond to an increase of 17% compared to the EE calculated based on the ZFO half-cells cycled between 0.01 V and 3.0 V. For even further pre-lithiated ZFO anodes (ZFO-600) the average EE is even further increased to 93%, as a consequence of the enhanced average CE (>99.7%) and VE (93%) (Fig. 4c). In fact, the obtained EE value is close to that of graphite-based full-cells with a theoretical LFP cathode (93.8%) [21]. Considering the high current used in the test, in fact, even higher EEs might be expected when cycling such cells at lower currents. The reason for this superior EE, especially in case of ZFO-600 is partially related to the relatively increased fraction of the alloying reaction as well as the capacity-limited cycling in general, as only a narrow operating voltage region of the anode is used (see inset in Fig. 4c). This shows that limiting the capacity has a complementary effect in addition to the relative increase of the alloying contribution, since both ZFO-deLi and ZFO-200 were cycled solely in the conversion regime, as indicated by the blue and green

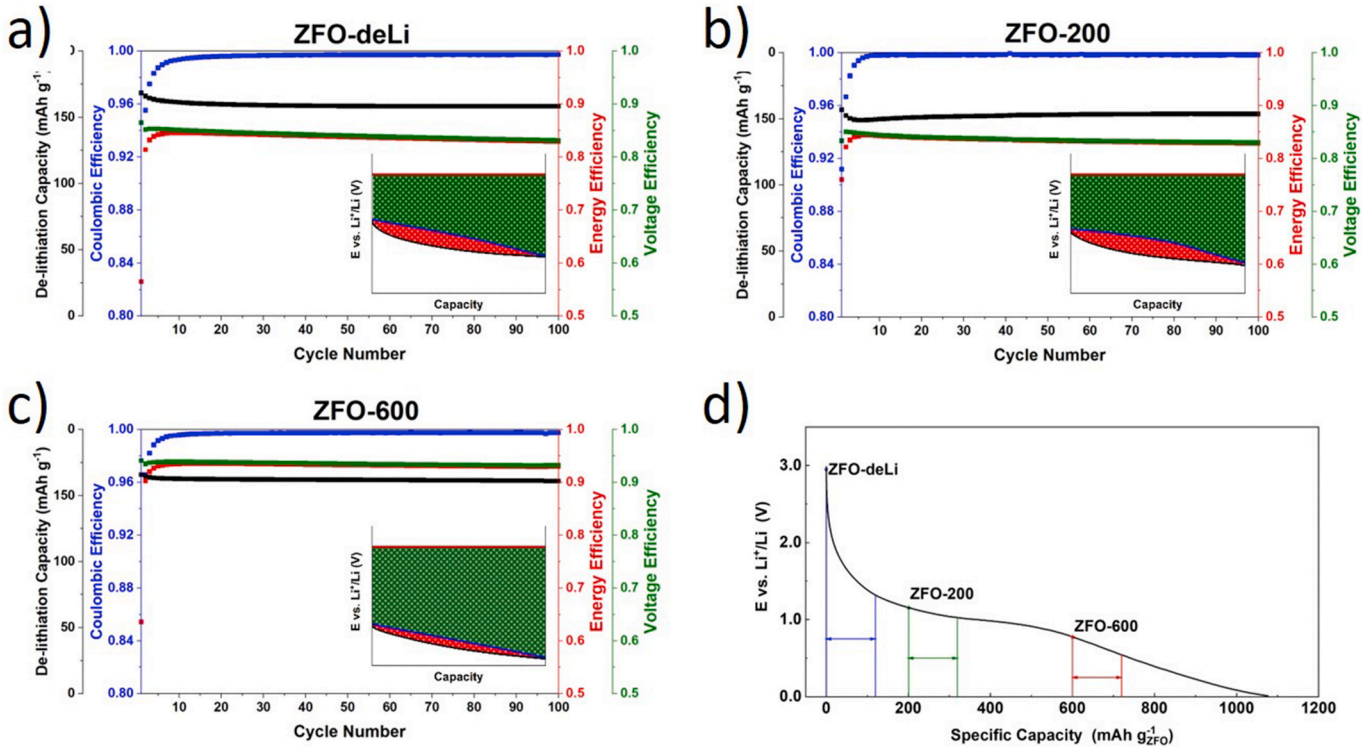

Fig. 4. Comparison of the de-/lithiation capacity, CE, VE, and EE plotted vs. the cycle number and representative dis-/charge profiles as inset for (a) ZFO-deLi/LFP_{exp}, (b) ZFO-200/LFP_{exp}, and (c) ZFO-600/LFP_{exp} full-cells. The anodes were pre-cycled and pre-lithiated as described in Section 4.4. The cells were cycled at a specific current of 2.45 A g^{-1}_{ZFO}. (d) Representative potential profile for the lithiation of ZFO, indicating the cycling range of the anode (ZFO-deLi, ZFO-200, and ZFO-600) for the three different full-cells depicted in (a–c).

region in Fig. 4d. From a practical point of view, this is a very important finding, as conventional lithium-ion batteries are always cathode-limited, in fact, while the use of the complete voltage range from 0.01 V to 3.0 V is not of practical relevance in any case with respect to the overall cell voltage.

4.5. *The influence of the cathode and its de-/lithiation potential*

As apparent from the discussion above, the VE and EE resulting from the use of an anode material can only be evaluated considering a positive electrode. LFP is frequently used, because it offers a very flat de-/lithiation potential at about 3.4 V, rendering this method generally applicable. The choice of the positive electrode active material, however, has a dramatic impact on the resulting VE and EE values. This effect is schematically illustrated in Fig. 5 for the transition from LFP_{theor} (ca. 3.4 V) to $LiNi_{0.5}Mn_{1.5}O_4$ ($LNMO_{theor}$; ca. 4.7 V [58]). As a matter of fact, considering this latter cathode material in combination with $Zn_{0.9}Fe_{0.1}O$, i.e., elevating the overall cell voltage by 1.3 V, while keeping all other parameters constant, increases the resulting EE by 9%, i.e., from 71% to 80%. The absolute value of energy "lost" remains the same, of course, but the reversibly stored energy increases. Hence, care has to be taken when simply comparing EE values in %.

To analyze this relationship more comprehensively for all CAMs studied herein, including the different cycling and pre-lithiation conditions, we calculated the dependency of the EE for varying positive electrode de-/lithiation potentials, ranging from 2.0 V (e.g., sulfur with a de-/lithiation potential of about 2.1 V [9,10]) to 5.0 V (e.g., $LiCoPO_4$ (LCP) with a de-/lithiation potential of about 4.85 V [59]). The results are shown in Fig. 6. Generally, as expected, the EE is increasing for all negative electrode active materials with an increasing de-/lithiation potential of the positive electrode. If the relative contribution of the alloying reaction is high, as for example in case of ZFO-600 or $Sn_{0.9}Fe_{0.1}O_2$-Cap.Lim., however, this increase is less pronounced compared to those negative electrodes that are characterized by a larger fraction of the conversion reaction, such as ZFO. This can be explained

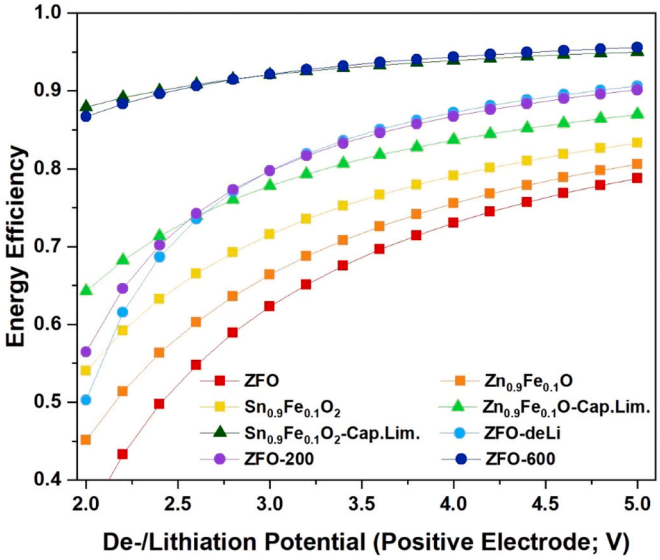

Fig. 6. Calculated energy efficiencies for the herein analyzed and investigated CAMs, including the different cycling and pre-lithiation conditions, as a function of the de-/lithiation potential of the positive electrode.

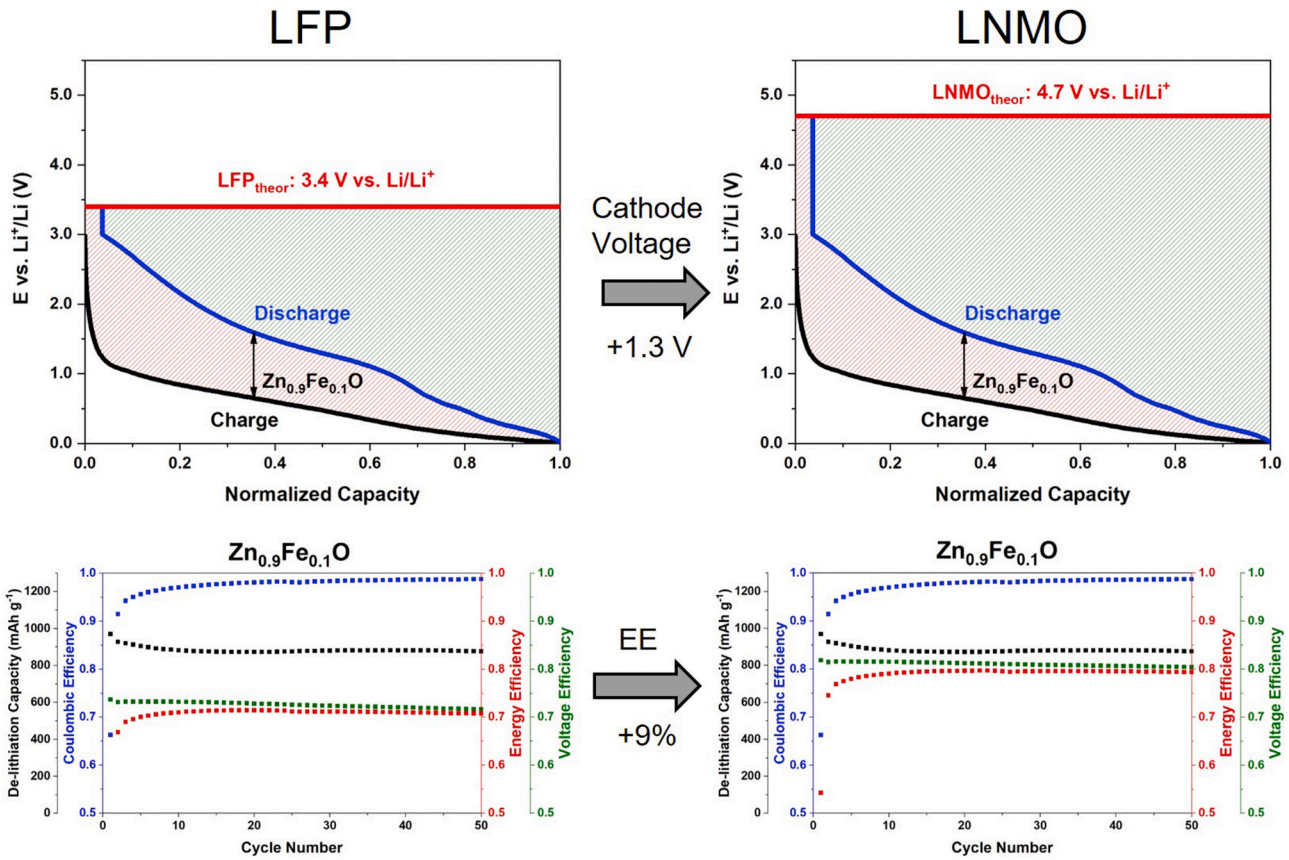

Fig. 5. Top: Schematic illustration of the EE for a (partially) theoretical lithium-ion cell comprised of an exemplary $Zn_{0.9}Fe_{0.1}O$-based anode and a LFP_{theor} (left-hand; 3.4 V) or $LNMO_{theor}$ (right-hand; 4.7 V) cathode. Bottom: The corresponding evaluation of the VE and EE for a $Zn_{0.9}Fe_{0.1}O$ negative electrode cycled in half-cell configuration – either with a LFP_{theor} (left-hand) or a $LNMO_{theor}$ (right-hand) positive electrode.

by the fact, that the alloying reaction occurs at lower potentials than the conversion reaction. If the anode operates at a rather high potential, the resulting voltage of the full-cell is low, especially if the cathode has a low de-/lithiation potential. Consequently, even a "small" voltage hysteresis decreases the EE significantly, since the reversibly stored energy is also small (relative to the "lost" energy) and the increase in EE with an increased cathode potential is more pronounced. As a general rule it can be said, that a higher de-/lithiation potential of the anode leads to a higher dependency of the EE on the de-/lithiation potential of the cathode. Remarkable is also the general trend that even for a cathode de-/lithiation potential of 5.0 V the anodes cycled with a limited capacity clearly outperform the anodes that have been cycled in a voltage range from 0.01 V to 3.0 V. Nonetheless, the highest EEs are observed when both measures are combined, i.e., increased contribution of the alloying reaction and limited capacity (ZFO-600 and $Sn_{0.9}Fe_{0.1}O_2$-Cap. Lim). The fact that the EE is less dependent on the de-/lithiation potential of the positive electrode is a clear advantage, indeed, as it renders the EE less dependent on the choice of the cathode chemistry. This is particularly important with respect to high-voltage cathodes such as LNMO or LCP, as continuous electrolyte decomposition at such high potentials has a negative effect on the CE and, thus, also the EE.

4.6. Comparison of (theoretical) gravimetric energy densities

CAMs generally provide high theoretical capacities – though within a rather large operational voltage window. Hence, high capacities do not always translate into high energy densities, as also confirmed by Badway et al. [60] for Co_3O_4/$LiCoO_2$ full-cells. In Table 1, we provide a calculation of theoretical gravimetric energy densities of lithium-ion cells comprising the anodes based on ZFO, $Zn_{0.9}Fe_{0.1}O$, $Sn_{0.9}Fe_{0.1}O_2$, $Zn_{0.9}Fe_{0.1}O$-Cap.Lim, as well as $Sn_{0.9}Fe_{0.1}O_2$-Cap.Lim. and a $LNMO_{theor}$ cathode with an average de-/lithiation potential of 4.7 V and a practical specific capacity of 140 mAh g^{-1} [58]. For comparison, we performed the same calculation for the corresponding lithium-ion cells with graphite as active material for the negative electrode, reflecting the state of the art [61]. Since commercial lithium-ion cells are commonly cathode-limited, we set the Q_c/Q_a ratio to 1/1, 1/1.1, and 1/1.2 to cover a certain range of different ratios. Note that we considered only the mass of the active materials in all cases for comparability reasons. Following the data provided in Table 1, the gravimetric energy density of the ZFO-based full-cells is the lowest, despite the high specific capacity. Nonetheless, it is increasing when elevating the contribution of the alloying reaction, i.e., switching from ZFO to $Zn_{0.9}Fe_{0.1}O$ or $Sn_{0.9}Fe_{0.1}O_2$, and further increasing when limiting the cycled capacity (i.e., for $Zn_{0.9}Fe_{0.1}O$-Cap.Lim. or $Sn_{0.9}Fe_{0.1}O_2$-Cap.Lim.), thus, approaching or even slightly surpassing the gravimetric energy density of graphite-based lithium-ion cells. We would like to note once again that the latter will require the design of scalable pre-lithiation processes. However, the results are remarkable considering the substantially better rate performance and, thus, (potential) power density of lithium-ion cells comprising CAMs as anode [33,36,50,51]. Interesting to note is the impact of decreasing the Q_c/Q_a ratio from 1/1 over 1/1.1 to 1/1.2 is less pronounced for high-capacity CAMs than for graphite. In the latter case, the gravimetric energy density decreases by about 5% each, whereas it is only around 2% in case of $Sn_{0.9}Fe_{0.1}O_2$, as simply less additional anode material (mass) is needed.

4.7. Evaluation of the (potential) performance in large cells

Based on the data and results presented in the previous paragraphs, we determined the impact of the EE on a practical battery of 22 kWh – a size that is suitable, e.g., for hybrid electric vehicles. As discussed above, the EE eventually determines the energy that is lost upon storage, causing additional cost and a detrimental effect on the overall sustainability of such device. Fig. 7a depicts the accumulated energy loss in % over 30 cycles for the 22 kWh CAM/$LNMO_{theor}$ full-cells and Fig. 7b displays the accumulated extra energy in kWh. For ZFO, the accumulated energy loss accounts for 659% and decreases to 629% and 550% for $Zn_{0.9}Fe_{0.1}O$ and $Sn_{0.9}Fe_{0.1}O_2$, respectively. These values are further reduced by capacity-limited cycling to 428% for $Zn_{0.9}Fe_{0.1}O$-Cap.Lim. and 175% for $Sn_{0.9}Fe_{0.1}O_2$-Cap.Lim. The value for $Sn_{0.9}Fe_{0.1}O_2$-Cap.Lim. is in a similar range as those reported for graphite and soft carbon based lithium-ion cells and certainly superior to lithium-ion cells containing an exemplary silicon/graphite composite as active material for the negative electrode [21] (note that the experimental design has been slightly different in the cited reference). Similarly, and in line with the EE data provided in Fig. 4, the accumulated energy loss for the pre-cycled and pre-lithiated ZFO/$LNMO_{theor}$ full-cells decreases for ZFO-deLi, ZFO-200, and ZFO-600 to 300%, 312%, and 143%, respectively. Compared to ZFO this means a reduction by over 50% for ZFO-deLi and ZFO-200 and more than 75% for ZFO-600.

For the accumulated extra energy needed to retain the 22 kWh over 30 cycles (Fig. 7b), this translates into 186 kWh for ZFO/$LNMO_{theor}$, 110 kWh for $Zn_{0.9}Fe_{0.1}O$-Cap.Lim./$LNMO_{theor}$, 41 kWh for $Sn_{0.9}Fe_{0.1}O_2$-Cap.Lim./$LNMO_{theor}$, and only 33 kWh in case of ZFO-600/$LNMO_{theor}$ – to provide just a few examples.

5. Summary and conclusions

In this work, we evaluated a series of CAMs as negative electrode in lithium-ion batteries with a particular focus on the energy efficiency (EE), which is commonly considered rather low, and potential measures to improve it. These measures include (i) an increase of the relative contribution of the alloying reaction, (ii) a limitation of the capacity cycled, (iii) pre-cycling and pre-lithiation of the anode, as well as (iv) the choice of the cathode material, precisely, its de-/lithiation potential. The results are summarized in Fig. 8, highlighting that a suitable combination of these measures allows for increasing the EE of such materials to a level that is comparable with the state-of-the-art anode, graphite. Specifically, an increase of the alloying contribution, potentially obtained

Table 1
Calculation of the gravimetric energy density of lithium-ion cells comprising different CAMs or graphite as anode active material and $LNMO_{theor}$ as active material for the cathode. The capacity values are based on commonly reported literature data. For the $LNMO_{theor}$ cathode, a specific capacity of 140 mAh g^{-1} was assumed and an average de-/lithiation potential of 4.7 V. The gravimetric energy density was calculated for different Q_c/Q_a ratios and based on the mass of the active materials only.

	Q_a/Q_c	Graphite	ZFO	$Zn_{0.9}Fe_{0.1}O$	$Sn_{0.9}Fe_{0.1}O_2$	$Zn_{0.9}Fe_{0.1}O$-Cap. Lim.	$Sn_{0.9}Fe_{0.1}O_2$–Cap. Lim.
Practical Capacity (mAh g^{-1})		360	1000	950	1600	600	600
Average Delithiation Potential *vs.* Li^+/Li (V)		0.2	1.55	1.3	1.2	1	0.55
Average Full-Cell Voltage (V)		4.5	3.15	3.4	3.5	3.7	4.15
Specific Energy (Wh kg^{-1})	1/1	454	387	415	439	420	471
Specific Energy (Wh kg^{-1})	1/1.1	441	382	410	434	412	462
Specific Energy (Wh kg^{-1})	1/1.2	430	378	404	430	405	454

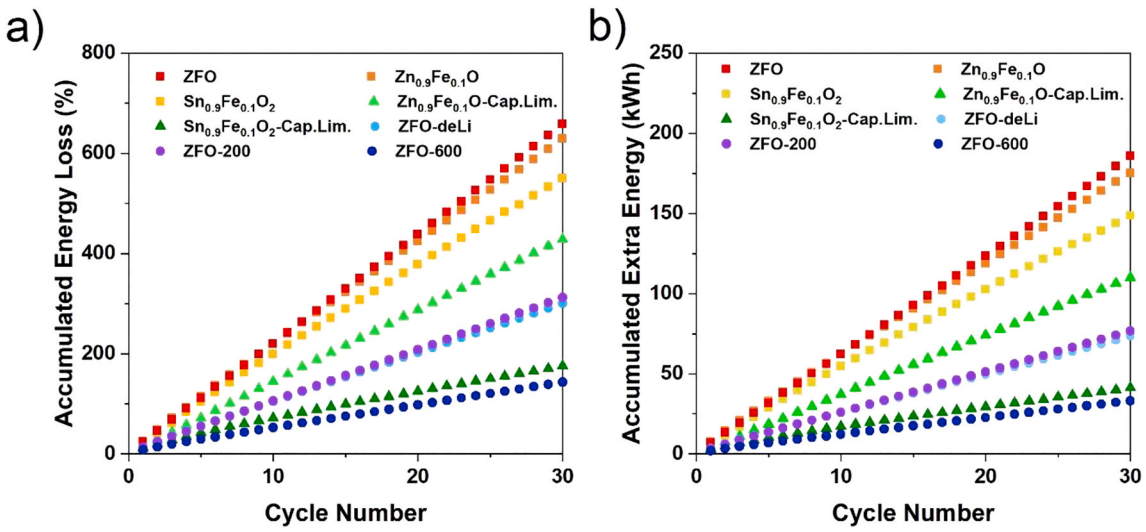

Fig. 7. Overview of the (a) accumulated energy loss in % for CAM/$LNMO_{theor}$ lithium-ion cells with a total energy of 22 kWh over 30 cycles. (b) The corresponding accumulated additional energy that is needed to retain the total energy of 22 kWh.

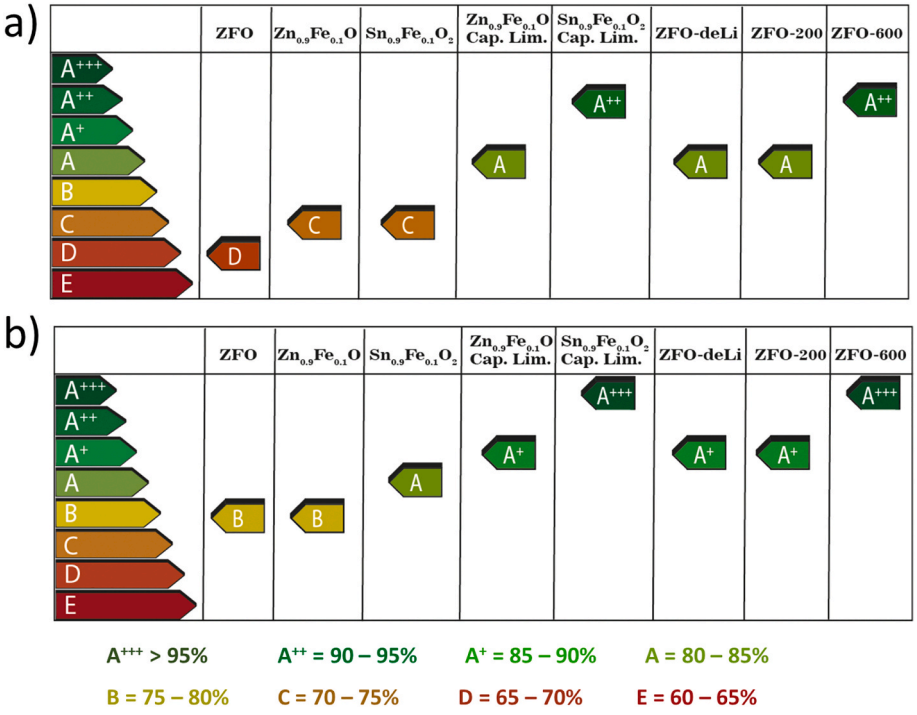

Fig. 8. Classification of the EE of the CAM negative electrodes investigated and analyzed herein, employing (a) LFP_{theor} or (b) $LNMO_{theor}$ as positive electrode, according to the European Union Energy Label.

via pre-lithiation and/or the choice of high-capacity alloying elements as two complementary approaches, in combination with high-voltage cathodes such as LNMO enables an EE of above 95%, labeled as A^{+++} in Fig. 8. Moreover, these materials may be employed in high-energy and high-power batteries that could be used, e.g., for hybrid electric vehicle batteries with limited energy loss upon cycling.

We may anticipate that these results will lead to a reconsideration of metal oxide anodes in lithium-ion batteries – especially, if the intense research and development efforts dedicated towards scalable pre-lithiation strategies will eventually allow for a commercialization of such technology.

Declaration of competing interest

The authors declare that they have no known competing financial interests or personal relationships that could have appeared to influence the work reported in this paper.

CRediT authorship contribution statement

Jakob Asenbauer: Data curation, Investigation, Writing - original draft. **Alberto Varzi:** Data curation, Resources, Writing - review & editing. **Stefano Passerini:** Conceptualization, Writing - review & editing. **Dominic Bresser:** Conceptualization, Funding acquisition, Writing - review & editing, Supervision.

Acknowledgement

The authors would like to thank the Vector Foundation within the NEW E^2 project as well as the Helmholtz Association for financial support.

References

[1] M. Armand, J.-M. Tarascon, Building better batteries, Nature 451 (2008) 652–657, https://doi.org/10.1038/451652a.
[2] B. Scrosati, J. Garche, Lithium batteries: status, prospects and future, J. Power Sources 195 (2010) 2419–2430.
[3] N. Nitta, G. Yushin, High-capacity anode materials for lithium-ion batteries: choice of elements and structures for active particles, Part. Part. Syst. Char. 31 (2014) 317–336, https://doi.org/10.1002/ppsc.201300231.
[4] M.R. Palacin, Recent advances in rechargeable battery materials: a chemist's perspective, Chem. Soc. Rev. 38 (2009) 2565–2575.
[5] J.B. Goodenough, How we made the Li-ion rechargeable battery, Nat. Electr. 1 (2018), https://doi.org/10.1038/s41928-018-0048-6, 204–204.
[6] M.S. Whittingham, Lithium batteries and cathode materials, Chem. Rev. 104 (2004) 4271–4302.
[7] B. Dunn, H. Kamath, J.-M. Tarascon, Electrical energy storage for the grid: a battery of choices, Science 334 (2011) 928–935.
[8] D. Bresser, K. Hosoi, D. Howell, H. Li, H. Zeisel, K. Amine, S. Passerini, Perspectives of automotive battery R&D in China, Germany, Japan, and the USA, J. Power Sources 382 (2018) 176–178, https://doi.org/10.1016/j.jpowsour.2018.02.039.
[9] D. Bresser, S. Passerini, B. Scrosati, Recent progress and remaining challenges in sulfur-based lithium secondary batteries - a review, Chem. Commun. 49 (2013) 10545–10562, https://doi.org/10.1039/C3CC46131A.
[10] A. Manthiram, Y. Fu, S.-H. Chung, C. Zu, Y.-S. Su, Rechargeable lithium–sulfur batteries, Chem. Rev. 114 (2014) 11751–11787, https://doi.org/10.1021/cr500062v.
[11] A.C. Luntz, B.D. McCloskey, Nonaqueous Li–air batteries: a status report, Chem. Rev. 114 (2014) 11721–11750, https://doi.org/10.1021/cr500054y.
[12] L. Grande, E. Paillard, J. Hassoun, J.-B. Park, Y.-J. Lee, Y.-K. Sun, S. Passerini, B. Scrosati, The lithium/air battery: still an emerging system or a practical reality? Adv. Mater. 27 (2015) 784–800, https://doi.org/10.1002/adma.201403064.
[13] C. Xia, C.Y. Kwok, L.F. Nazar, A high-energy-density lithium-oxygen battery based on a reversible four-electron conversion to lithium oxide, Science 361 (2018) 777, https://doi.org/10.1126/science.aas9343.
[14] P. Poizot, S. Laruelle, S. Grugeon, L. Dupont, J.-M. Tarascon, Nano-sized transition-metal oxides as negative-electrode materials for lithium-ion batteries, Nature 407 (2000) 496–499, https://doi.org/10.1038/35035045.
[15] S. Fang, D. Bresser, S. Passerini, Transition metal oxide anodes for electrochemical energy storage in lithium- and sodium-ion batteries, Adv. Energy Mater. 10 (2020), 1902485, https://doi.org/10.1002/aenm.201902485.
[16] J. Cabana, L. Monconduit, D. Larcher, M.R. Palacín, Beyond intercalation-based Li-ion batteries: the state of the art and challenges of electrode materials reacting through conversion reactions, Adv. Mater. 22 (2010) E170–E192, https://doi.org/10.1002/adma.201000717.
[17] D. Bresser, S. Passerini, B. Scrosati, Leveraging valuable synergies by combining alloying and conversion for lithium-ion anodes, Energy Environ. Sci. 9 (2016) 3348–3367, https://doi.org/10.1039/c6ee02346k.
[18] G.A. Elia, J. Hassoun, W.-J. Kwak, Y.-K. Sun, B. Scrosati, F. Mueller, D. Bresser, S. Passerini, P. Oberhumer, N. Tsiouvaras, J. Reiter, An advanced lithium–air battery exploiting an ionic liquid-based electrolyte, Nano Lett. 14 (2014) 6572–6577, https://doi.org/10.1021/nl5031985.
[19] P.J. Kim, S. Narayanan, J. Xue, V. Thangadurai, V.G. Pol, Li-Ion-Permeable and electronically conductive membrane comprising garnet-type Li6La3Ta1.5Y0.5O12 and graphene toward ultrastable and high-rate lithium sulfur batteries, ACS Appl. Energy Mater. 1 (2018) 3733–3741, https://doi.org/10.1021/acsaem.8b00519.
[20] A. Eftekhari, Energy efficiency: a critically important but neglected factor in battery research, Sustain. Energy Fuels 1 (2017) 2053–2060, https://doi.org/10.1039/C7SE00350A.
[21] P. Meister, H. Jia, J. Li, R. Kloepsch, M. Winter, T. Placke, Best practice: performance and cost evaluation of lithium ion battery active materials with special emphasis on energy efficiency, Chem. Mater. 28 (2016) 7203–7217, https://doi.org/10.1021/acs.chemmater.6b02895.
[22] W. Dreyer, J. Jamnik, C. Guhlke, R. Huth, J. Moskon, M. Gaberscek, The thermodynamic origin of hysteresis in insertion batteries, Nat. Mater. 9 (2010) 448–453, https://doi.org/10.1038/nmat2730.
[23] J. Asenbauer, A. Hoefling, S. Indris, J. Tübke, S. Passerini, D. Bresser, Mechanistic insights into the lithiation and delithiation of iron-doped zinc oxide: the nucleation site model, ACS Appl. Mater. Interfaces 12 (2020) 8206–8218, https://doi.org/10.1021/acsami.9b19958.
[24] R.E. Doe, K.A. Persson, Y.S. Meng, G. Ceder, First-principles investigation of the Li Fe F phase diagram and equilibrium and nonequilibrium conversion reactions of iron fluorides with lithium, Chem. Mater. 20 (2008) 5274–5283, https://doi.org/10.1021/cm801105p.
[25] A. Ponrouch, J. Cabana, R. Dugas, J.L. Slack, M.R. Palacín, Electroanalytical study of the viability of conversion reactions as energy storage mechanisms, RSC Adv. 4 (2014) 35988–35996, https://doi.org/10.1039/C4RA05189K.
[26] F. Mestre-Aizpurua, S. Laruelle, S. Grugeon, J.-M. Tarascon, M.R. Palacín, High temperature lithium cells using conversion oxide electrodes, J. Appl. Electrochem. 40 (2010) 1365–1370, https://doi.org/10.1007/s10800-010-0103-0.
[27] P.L. Taberna, S. Mitra, P. Poizot, P. Simon, J.-M. Tarascon, High rate capabilities Fe3O4-based Cu nano-architectured electrodes for lithium-ion battery applications, Nat. Mater. 5 (2006) 567–573, https://doi.org/10.1038/nmat1672.
[28] Y. Oumellal, A. Rougier, G.A. Nazri, J.-M. Tarascon, L. Aymard, Metal hydrides for lithium-ion batteries, Nat. Mater. 7 (2008) 916–921, https://doi.org/10.1038/nmat2288.
[29] M.N. Obrovac, V.L. Chevrier, Alloy negative electrodes for Li-ion batteries, Chem. Rev. 114 (2014) 11444–11502, https://doi.org/10.1021/cr500207g.
[30] C.-M. Park, J.-H. Kim, H. Kim, H.-J. Sohn, Li-alloy based anode materials for Li secondary batteries, Chem. Soc. Rev. 39 (2010) 3115–3141, https://doi.org/10.1039/B919877F.
[31] W.-J. Zhang, A review of the electrochemical performance of alloy anodes for lithium-ion batteries, J. Power Sources 196 (2011) 13–24, https://doi.org/10.1016/j.jpowsour.2010.07.020.
[32] V.L. Chevrier, J.R. Dahn, First principles studies of disordered lithiated silicon, J. Electrochem. Soc. 157 (2010) A392, https://doi.org/10.1149/1.3294772.
[33] A. Varzi, D. Bresser, J. von Zamory, F. Mueller, S. Passerini, ZnFe2O4-C/LiFePO4-CNT: a novel high power lithium-ion battery with excellent cycling performance, Adv. Energy Mater. 4 (2014), 1400054, https://doi.org/10.1002/aenm.201400054.
[34] D. Bresser, F. Mueller, M. Fiedler, S. Krueger, R. Kloepsch, D. Baither, M. Winter, E. Paillard, S. Passerini, Transition metal doped zinc oxide nanoparticles as new lithium-ion anode material, Chem. Mater. 25 (2013) 4977–4985, https://doi.org/10.1021/cm403443t.
[35] F. Mueller, D. Geiger, U. Kaiser, S. Passerini, D. Bresser, Elucidating the impact of cobalt-doping on the lithium storage mechanism in conversion/alloying-type zinc oxide anodes, ChemElectroChem 3 (2016) 1311–1319, https://doi.org/10.1002/celc.201600179.
[36] J. Asenbauer, J.R. Binder, F. Mueller, M. Künzel, D. Geiger, U. Kaiser, S. Passerini, D. Bresser, Scalable synthesis of micro-sized nanocrystalline Zn0.9Fe0.1O-C secondary particles and their use in Zn0.9Fe0.1O-C/LiNi0.5Mn1.5O4 lithium-ion full-cells, ChemSusChem (2020), https://doi.org/10.1002/cssc.202000559.
[37] H. Chen, T.N. Cong, W. Yang, C. Tan, Y. Li, Y. Ding, Progress in electrical energy storage system: a critical review, Prog. Nat. Sci. 19 (2009) 291–312, https://doi.org/10.1016/j.pnsc.2008.07.014.
[38] D. Bresser, E. Paillard, R. Kloepsch, S. Krueger, M. Fiedler, R. Schmitz, D. Baither, M. Winter, S. Passerini, Carbon coated ZnFe2O4 nanoparticles for advanced lithium-ion anodes, Adv. Energy Mater. 3 (2013) 513–523, https://doi.org/10.1002/aenm.201200735.
[39] F. Mueller, D. Bresser, V.S.K. Chakrayadhanula, S. Passerini, Fe-doped SnO2 nanoparticles as new high capacity anode material for secondary lithium-ion batteries, J. Power Sources 299 (2015) 398–402, https://doi.org/10.1016/j.powsour.2015.08.018.
[40] F. Mueller, D. Bresser, E. Paillard, M. Winter, S. Passerini, Influence of the carbonaceous conductive network on the electrochemical performance of ZnFe2O4 nanoparticles, J. Power Sources 236 (2013) 87–94, https://doi.org/10.1016/j.jpowsour.2013.02.051.
[41] F. Martinez-Julian, A. Guerrero, M. Haro, J. Bisquert, D. Bresser, E. Paillard, S. Passerini, G. Garcia-Belmonte, Probing lithiation kinetics of carbon-coated ZnFe2O4 nanoparticle battery anodes, J. Phys. Chem. C 118 (2014) 6069–6076, https://doi.org/10.1021/jp412641v.
[42] A. Di Cicco, A. Giglia, R. Gunnella, S.L. Koch, F. Mueller, F. Nobili, M. Pasqualini, S. Passerini, R. Tossici, A. Witkowska, SEI growth and depth profiling on ZFO electrodes by soft X-ray absorption spectroscopy, Adv. Energy Mater. 5 (2015), 1500642, https://doi.org/10.1002/aenm.201500642.
[43] S.J. Rezvani, Y. Mijiti, R. Gunnella, F. Nobili, A. Trapananti, M. Minicucci, M. Ciambezi, D. Bresser, S. Nannarone, S. Passerini, A. Di Cicco, Structure rearrangements induced by lithium insertion in metal alloying oxide mixed spinel structure studied by x-ray absorption near-edge spectroscopy, J. Phys. Chem. Solid. 136 (2020), 109172, https://doi.org/10.1016/j.jpcs.2019.109172.
[44] S.J. Rezvani, M. Ciambezi, R. Gunnella, M. Minicucci, M.A. Muñoz-Márquez, F. Nobili, M. Pasqualini, S. Passerini, C. Schreiner, A. Trapananti, A. Witkowska, A. Di Cicco, Local structure and stability of SEI in graphite and ZFO electrodes probed by as K-edge absorption spectroscopy, J. Phys. Chem. C 120 (2016) 4287–4295, https://doi.org/10.1021/acs.jpcc.5b11798.
[45] S.J. Rezvani, R. Gunnella, A. Witkowska, F. Mueller, M. Pasqualini, F. Nobili, S. Passerini, A.D. Cicco, Is the solid electrolyte interphase an extra-charge reservoir in Li-ion batteries? ACS Appl. Mater. Interfaces 9 (2017) 4570–4576, https://doi.org/10.1021/acsami.6b12408.
[46] M. Ciambezi, A. Trapananti, S.J. Rezvani, F. Maroni, D. Bresser, M. Minicucci, F. Nobili, R. Gunnella, S. Passerini, A. Di Cicco, Initial lithiation of carbon-coated zinc ferrite anodes studied by in-situ X-ray absorption spectroscopy, Radiat. Phys. Chem. (2019), 108468, https://doi.org/10.1016/j.radphyschem.2019.108468.
[47] F. Mueller, A. Gutsche, H. Nirschl, D. Geiger, U. Kaiser, D. Bresser, S. Passerini, Iron-doped ZnO for lithium-ion anodes: impact of the dopant ratio and carbon coating content, J. Electrochem. Soc. 164 (2017) A6123–A6130, https://doi.org/10.1149/2.0171701jes.

[48] G. Giuli, A. Trapananti, F. Mueller, D. Bresser, F. d'Acapito, S. Passerini, Insights into the effect of iron and cobalt doping on the structure of nanosized ZnO, Inorg. Chem. 54 (2015) 9393–9400, https://doi.org/10.1021/acs.inorgchem.5b00493.
[49] L. Cabo-Fernandez, D. Bresser, F. Braga, S. Passerini, L.J. Hardwick, In-Situ electrochemical SHINERS investigation of SEI composition on carbon-coated Zn0.9Fe0.1O anode for lithium-ion batteries, Batteries Supercaps 2 (2019) 168–177, https://doi.org/10.1002/batt.201800063.
[50] Y. Ma, Y. Ma, G. Giuli, T. Diemant, R.J. Behm, D. Geiger, U. Kaiser, U. Ulissi, S. Passerini, D. Bresser, Conversion/alloying lithium-ion anodes – enhancing the energy density by transition metal doping, Sustain. Energy Fuels 2 (2018) 2601–2608, https://doi.org/10.1039/C8SE00424B.
[51] A. Birrozzi, J. Asenbauer, T.E. Ashton, A.R. Groves, D. Geiger, U. Kaiser, J.A. Darr, D. Bresser, Tailoring the charge/discharge potentials and electrochemical performance of SnO2 lithium-ion anodes by transition metal Co-doping, Batteries Supercaps 3 (2020) 284–292, https://doi.org/10.1002/batt.201900154.
[52] K. Naoi, P. Simon, New materials and new configurations for advanced electrochemical capacitors, Electrochem. Soc. Interf. 17 (2008) 34–37.
[53] A. Burke, R&D considerations for the performance and application of electrochemical capacitors, Electrochim. Acta 53 (2007) 1083–1091, https://doi.org/10.1016/j.electacta.2007.01.011.
[54] P. Simon, Y. Gogotsi, Materials for electrochemical capacitors, Nat. Mater. 7 (2008) 845–854, https://doi.org/10.1038/nmat2297.
[55] V.L. Chevrier, L. Liu, R. Wohl, A. Chandrasoma, J.A. Vega, K.W. Eberman, P. Stegmaier, E. Figgemeier, Design and testing of prelithiated full cells with high silicon content, J. Electrochem. Soc. 165 (2018) A1129–A1136, https://doi.org/10.1149/2.1161805jes.
[56] V. Aravindan, Y.-S. Lee, S. Madhavi, Best practices for mitigating irreversible capacity loss of negative electrodes in Li-ion batteries, Adv. Energy Mater. 7 (2017), 1602607, https://doi.org/10.1002/aenm.201602607.
[57] F. Holtstiege, P. Baermann, R. Noelle, M. Winter, T. Placke, Pre-lithiation strategies for rechargeable energy storage technologies: concepts, promises and challenges, Batteries 4 (2018) 4–42.
[58] S. Patoux, L. Sannier, H. Lignier, Y. Reynier, C. Bourbon, S. Jouanneau, F. Le Cras, S. Martinet, High voltage nickel manganese spinel oxides for Li-ion batteries, Electrochim. Acta 53 (2008) 4137–4145, https://doi.org/10.1016/j.electacta.2007.12.054.
[59] N. Laszczynski, A. Birrozzi, K. Maranski, M. Copley, M.E. Schuster, S. Passerini, Effect of coatings on the green electrode processing and cycling behaviour of LiCoPO4, J. Mater. Chem. A. 4 (2016) 17121–17128, https://doi.org/10.1039/C6TA05262B.
[60] F. Badway, I. Plitz, S. Grugeon, S. Laruelle, M. Dollé, A.S. Gozdz, J.-M. Tarascon, Metal oxides as negative electrode materials in Li-ion cells, Electrochem. Solid State Lett. 5 (2002) A115–A118, https://doi.org/10.1149/1.1472303.
[61] N. Loeffler, D. Bresser, S. Passerini, M. Copley, Secondary lithium-ion battery anodes - from first commercial batteries to recent research activities, Johnson Matthey Technol. Rev. 59 (2015) 34–44, https://doi.org/10.1595/205651314X685824.